

Joint Reconstruction of Spatially-Coherent and Realistic Clothed Humans and Objects from a Single Image

Ayushi Dutta* Marco Pesavento* Marco Volino Adrian Hilton
Armin Mustafa

Centre for Vision, Speech and Signal Processing (CVSSP), University of Surrey, Guildford, UK

{a.dutta, m.pesavento, m.volino, a.hilton, a.mustafa}@surrey.ac.uk

Abstract

Recent advances in human shape learning have focused on achieving accurate human reconstruction from single-view images. However, in the real world, humans share space with other objects. Reconstructing images with humans and objects is challenging due to the occlusions and lack of 3D spatial awareness, which leads to depth ambiguity in the reconstruction. Existing methods in monocular human-object reconstruction fail to capture intricate details of clothed human bodies and object surfaces due to their template-based nature. In this paper, we jointly reconstruct clothed humans and objects in a spatially coherent manner from single-view images, while addressing human-object occlusions. A novel attention-based neural implicit model is proposed that leverages image pixel alignment to retrieve high-quality details, and incorporates semantic features extracted from the human-object pose to enable 3D spatial awareness. A generative diffusion model is used to handle human-object occlusions. For training and evaluation, we introduce a synthetic dataset with rendered scenes of inter-occluded 3D human scans and diverse objects. Extensive evaluation on both synthetic and real datasets demonstrates the superior quality of proposed human-object reconstructions over competitive methods.

1. Introduction

In recent years, there has been a growing demand for digitizing 3D humans and objects for applications ranging from virtual reality, movie production, gaming and social telepresence. Research has moved towards obtaining high-quality surface details of either clothed humans [7, 8, 22, 29, 41] or textured objects [1, 3, 6, 33, 45] from single-view images. Since most existing methods focus solely on either human or object reconstruction, they perceive humans and objects in isolation, whereas real images generally contain both humans and objects in the same scene. Recent

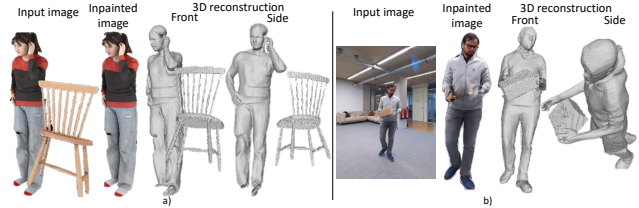


Figure 1. SCHOR jointly reconstructs spatially coherent realistic clothed humans and objects from synthetic (a) and real (b) images by first handling occlusion with a conditioned generative model followed by attention-based neural implicit model estimation.

works [20, 36–38, 47] have reconstructed humans and objects jointly, but they rely on parametric template-based representations, which limit realism, failing to capture loose clothing, complex hairstyles, and the free-form shapes of objects. In this paper, for the first time, we jointly reconstruct realistic, non-parametric clothed humans and objects from single images, in a spatially coherent way, addressing the gap in the literature.

Single-view 3D reconstruction of human and object scenes is an inherently ill-posed problem. Multiple 3D spatial configurations of humans and objects can project to the same 2D image, leading to depth ambiguity and difficulty in estimating the relative size, shape and position of the human-object in the 3D space. Human-object occlusion further complicates the inference. Previous methods solve this by using parametric models [47] to enforce geometric and spatial constraints to predict the 3D spatial arrangement. However, they do not achieve realistic 3D human-object reconstruction, because this also requires recovering fine details in both visible and occluded regions, increasing the task complexity.

To address these challenges, we propose SCHOR, a novel framework that can jointly produce Spatially-Coherent realistic Human Object Reconstructions from a single image, as shown in Fig. 1. This is achieved by introducing a novel attention-based neural implicit model that estimates the implicit representation of both humans and objects. Unlike parametric representations, the implicit representation en-

*Equal contribution

hances the realism of the reconstruction because the proposed implicit model leverages local pixel-aligned features extracted from a full-body human image and a segmented object image. Because the human is likely occluded by the object, the full-body human image is created by inpainting the non-visible body regions of the segmented partial human image using a generative model, allowing the implicit model to reproduce details in the body regions occluded by the object. To ensure 3D spatial coherence, the neural implicit model uses self-attention to incorporate global context from the input human-object RGB image as well as semantic features from a human-object pose estimated from the image. As a result, SCHOR can jointly reason about the 3D human-object spatial configuration while also retrieving high-quality details in the reconstruction.

Due to the lack of existing datasets with high-quality, ground-truth 3D surfaces for human-object scenes, we created synHOR, a synthetic dataset for Human Object Reconstruction to train and evaluate SCHOR. We simulate human-object scenes by randomly placing 3D human scans from the public THuman2.0 [44] dataset with selected 3D object meshes from BEHAVE [2] and HODome [46] datasets, in a variety of 3D spatial configurations. We also evaluate our model on the real-world BEHAVE [2] dataset and demonstrate superior performance of reconstructions against state-of-the-art methods. Our key contributions include:

- We introduce a novel framework to jointly reconstruct spatially coherent, realistic human-object shapes from single images. To the best of our knowledge, this is the first work towards achieving realistic non-parametric human-object reconstructions from single images.
- We propose a novel attention-based neural implicit network that jointly reasons about the 3D human-object locations and retrieves realistic human surface details and object shapes.
- We demonstrate superior human-object reconstruction quality compared to the state-of-the-art methods, both quantitatively and qualitatively, on synthetic and real datasets.

2. Related works

3D human and object reconstruction: To reconstruct 3D human and object jointly, previous methods use parametric models to fit human and object meshes satisfying various human-object interaction constraints. PHOSA [47] and D3D-HOI [43] each proposed an optimization based framework with physical constraints on scale and predefined contact priors. Wang *et al.* [35] modeled 3D human-object interactions from an image using commonsense knowledge from large language models. Holistic++ [4] modeled fine-grained human-object relations in a scene and inferred using Markov chain Monte Carlo method. CHORE proposed the learning of neural-implicit functions and then fit parametric

model to the learned representation. Vistracker [37], InterTrack [39] reconstruct single human-object from a video, by specifically modeling the temporal context. Recently, CONTHO [20] proposed a method to refine human-object reconstruction from an image by 3D guided contact estimation. ProciGen [38] designed a framework to synthetically generate a large diverse dataset, and proposed a Hierarchical Diffusion Model to reconstruct human and object. None of the current approaches focused on single-view human-object reconstruction are able to recover clothed human subjects at the same fidelity as SCHOR. Alternate methods [9, 10, 31, 46] that can reconstruct clothed human-object, either use sparse or multi-views or monocular RGBD image as inputs, thereby relaxing their constraints and are thus not comparable to our work. We address the problem of jointly reconstructing realistic non-parametric clothed humans and objects from single images. **Neural implicit model for single-view 3D:** Early reconstruction methods cannot produce high-quality 3D shapes, which limits the realism of reconstructions. This arises from the discretized nature of traditional representations like voxels, meshes or point clouds. The ground-breaking introduction of the implicit representation for 3D reconstruction [5, 19, 21] leads deep learning approaches to adopt this continuous form of representation because it can represent fine-scale details on the reconstructed surfaces. These methods employ neural implicit models to estimate the implicit representation of 3D points in space.

Several works have since used neural implicit models for object reconstruction from single images. Early models estimate occupancy [5, 19] or signed distance fields [21, 42, 49] using multi-layer perceptrons (MLPs) that are conditioned on input features. More recent works modify this basic architecture to improve the object reconstruction by incorporating prior knowledge into implicit functions [3, 16]; using monocular geometric cues [45]; combining explicit templates with implicit representations [6, 33] or leveraging input global and local features [1, 14].

Another line of neural implicit models focuses on reconstructing high-quality 3D human shapes from single images. PIFu [28] introduced the pixel-alignment implicit function, which enhanced the level of detail of the 3D human shape. Building on pixel alignment, several methods have been developed to further improve detail quality using normal maps [29, 40] or super-resolution shapes [22]; addressing depth ambiguity using parametric models [7, 50]; and achieving complete reconstructions with diffusion models [8, 12, 30] or by incorporating additional data such as depth maps [23, 41] or unconstrained images [24]

However, these approaches cannot jointly reconstruct both human and object shapes and are generally category-specific, with human-focused methods unable to reconstruct objects and object-focused methods unable to reconstruct

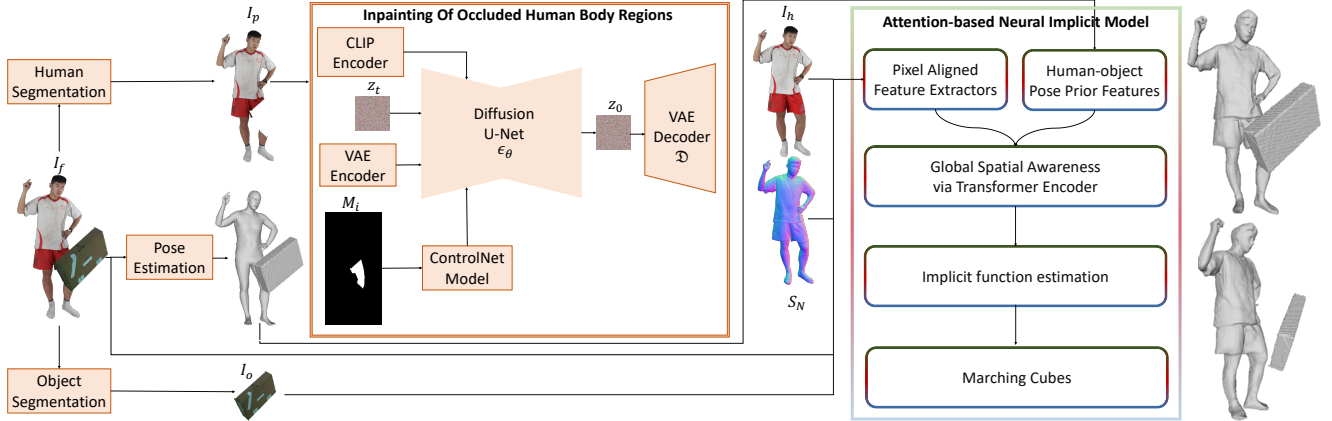


Figure 2. SCHOR overview: Given an input image of a human-object scene, we first use a generative model to inpaint occluded human body regions, guided by a mask of missing areas and the segmented input of the human. Next, the generated image, along with an estimated normal map, the input image, the segmented object image, and estimated pose parameters, are processed by an attention-based neural implicit model. This model jointly estimates the implicit representation of the human-object shape.

human shapes. Our proposed approach enables spatially coherent and realistic joint reconstruction of clothed humans and objects from a single image.

3. Spatially-coherent, realistic 3D shapes of clothed humans and objects

Overview: Recent methods for modeling human-object interactions, rely on template-based parametric representations that lack high-quality details, such as clothing and wrinkles, reducing the realism of the reconstruction. Other works that aim to achieve high-quality 3D shapes are mostly category-specific (either object or human) and cannot jointly reconstruct human-object shapes. To address these challenges, we introduce a novel framework that takes an RGB image as input and achieves Spatial-Coherent, realistic clothed Humans and Objects Reconstructions (SCHOR). In the proposed pipeline, shown in Fig. 2, the image is first segmented to separate the human from the object, and pose parameters of the SMPL-H [27] model are estimated. Occlusion is then addressed using the generative power of an image-conditioned diffusion model, which inpaints occluded regions of the human body. Implicit representations of both the human s_h and the object s_o are then estimated using a novel attention-based neural implicit model that incorporates the input RGB image I_f , the generated full-body human image I_h , the object image I_o and the estimated pose parameters. Compared to related works, our approach jointly reconstructs realistic clothed humans and objects while preserving 3D spatial coherence between them.

3.1. Inpainting of occluded human body regions

This work addresses cases in real images where the human is occluded by an object. When such occlusion happens, regions of the human body are missing in the input image, leaving the neural implicit model without the informa-

tion needed to estimate these regions. We propose to leverage the generative capability of diffusion models to inpaint the occluded body regions, using the partial human image I_p along with a mask of the occluded regions M_i . Given the input image I_f , we first apply semantic segmentation to separate the human from the object, while estimating SMPL-H [27] poses for both. Using the SMPL-H model, we then generate a mask of the human M_s , and we obtain the human-object intersection mask M_i as $M_i = M_s - M_p$, where M_p is the segmented partial human mask. Inspired by SiTH [8], we leverage an image-condition latent diffusion model [26] (LDM) to learn the conditional distribution of the missing human body regions. Rather than training the LDM from scratch, we adopt a fine-tuning strategy [13, 48] that optimizes the cross-attention layers of a pretrained diffusion U-Net [26]. The learning is conditioned using a ControlNet [48], which processes M_i to guide the generation. Additionally, we condition the U-Net with features from the partial human image I_p , extracted via a pre-trained CLIP [25] image encoder and a VAE encoder ε , to ensure that the generated image I_h matches the appearance of I_p . These features, along with randomly sampled noise ϵ , are input to the LDM model ϵ_θ , conditioned by the ControlNet, which generates a latent code z within the VAE latent distribution $z = \varepsilon(I_h^{gt})$, where I_h^{gt} is the ground-truth full-body human image. The output full-body image I_h is then generated by decoding with the VAE decoder \mathcal{D} a latent code \tilde{z} derived through iterative denoising of Gaussian noise: $I_h = \mathcal{D}(\tilde{z})$.

We define the objective function for fine-tuning as:

$$\min_{\theta} \mathbb{E}_{z \sim \varepsilon(I_h^{gt}), t, \epsilon \sim \mathcal{N}(\mathbf{0}, \mathbf{I})} \|\epsilon - \epsilon_\theta(z_t, t, I_p, M_i)\|_2^2 \quad (1)$$

The ground-truth latent code $z_0 = \varepsilon(I_h^{gt})$ is diffused over t time steps, resulting in the noisy latent z_t . The image-conditioned LDM model ϵ_θ predicts the noise ϵ added to the noisy latent z_t , based on time step $t \sim [0, 1000]$ and

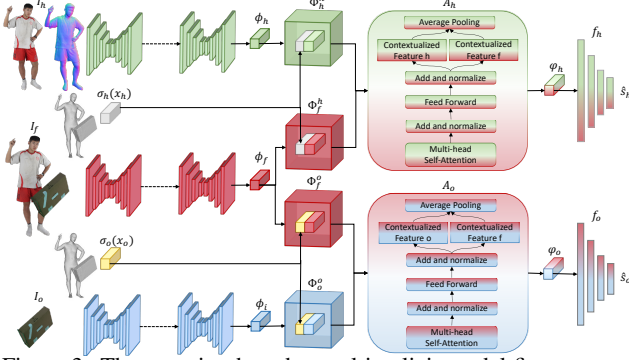


Figure 3. The attention-based neural implicit model first extracts pixel-aligned features from the input images to capture local high-frequency details. It then uses a transformer encoder to merge these features, achieving 3D spatial awareness. Finally, the model estimates the implicit representations for both humans and objects.

conditional inputs I_p and M_i .

To inpaint the occluded body regions during inference, we generate a latent \tilde{z}_0 by starting with Gaussian noise $z_T \sim \mathcal{N}(\mathbf{0}, \mathbf{I})$ and using an iterative denoising process. The final full-body image I_h is obtained with the decoder \mathcal{D} :

$$I_h = \mathcal{D}(\tilde{z}_0) = \mathcal{D}(f_\theta(z_T, I_h, M_i)) \quad (2)$$

where f_θ indicates the iterative denoising process of ϵ_θ . Finally, a 2D normal map S_N is estimated from I_h and concatenated with it. For simplicity, we continue to refer to this concatenated result as I_h throughout the paper.

3.2. Attention-based neural implicit model

To reconstruct the 3D shapes of both humans and objects, we introduce a novel attention-based neural implicit model that jointly estimates their implicit representations. This model aims to estimate an implicit representation that defines a surface as the level set of a function f , i.e. $f(X) = 0$ where X is a set of 3D points in \mathbb{R}^3 . The reconstructed surface is then defined as the zero level-set of f :

$$f' = \{x : f(x) = 0, x \in \mathbb{R}^3\} \quad (3)$$

The proposed implicit model comprises of multiple modules, as shown in Fig. 3

Pixel-aligned feature extractors: Previous methods on 3D human reconstruction [22, 28, 29] demonstrate that projecting a 3D point $x \in \mathbb{R}^3$ in the embedded image feature space $\phi(I)$ extracted with a convolutional stacked hour-glass network significantly increases the quality of 3D human shapes. SCHOR first extracts a feature embedding for each input image $\phi_{\{h,o,f\}}(I_{\{h,o,f\}})$. A first set of points X_h is then projected onto I_f and I_h via perspective projection π and linked to the corresponding features ϕ_h and ϕ_f to obtain pixel-alignment with the human: $\Phi_{\{h,f\}}^h = \phi_{\{h,f\}}(\pi(X_h, I_{\{h,f\}}))$. Similarly, the pixel-aligned object features $\Phi_{\{o,f\}}^o = \phi_{\{o,f\}}(\pi(X_o, I_{\{o,f\}}))$ are obtained by projecting a different set of points X_o on I_o and I_f and indexing them with the corresponding features ϕ_o and ϕ_f .

Human-object pose prior features: To guide the 3D reconstruction, we use geometric priors from an initial SMPL-H and object mesh estimated from the input image. Following previous work [20, 36, 37], our method initializes the object pose from a given object template. To define the pose features, for a query point $x_h \in X_h$, we look for the closest point x_h^* on SMPL-H, i.e. $x_h^* = \arg \min_{x_h^p} \|x_h - x_h^p\|$ where x_h^p are points on the SMPL-H mesh. Our human pose prior features $\sigma_h(x_h) = [d_h, v_h, z_h]$ then constitutes three elements: a signed distance value d_h between x_h and x_h^* , a visibility label $v_h \in \{1, 0\}$ where v_h indicates if x_h^* is visible in the front image when SMPL-H and initial object mesh is projected together, and a relative depth-aware feature $z_h = (x_h^z - z_c)$ where z_c is the depth of the SMPL-H centre and x_h^z is the depth of the query point x_h . Analogously, for a query point $x_o \in X_o$ and its closest point on the object mesh, x_o^* , the object pose prior features $\sigma_o(x_o) = [d_o, v_o, z_o]$ also constitutes three elements: a signed distance value d_o between x_o and x_o^* , a visibility label $v_o \in \{1, 0\}$ and a relative depth-aware feature $z_o = (x_o^z - z_c)$ where x_o^z is the depth of the query point x_o . The object position is also defined relative to the SMPL-H centre, to learn 3D spatial coherency with the human.

Global spatial awareness via transformer encoders: as shown in Sec. 4.1, simply concatenating the features of the human Φ_h^h and object Φ_o^o with those of the input image $\Phi_f^{\{h,o\}}$ deteriorates network performance, making it less robust to noise of the input image. Additionally, the network’s ability to integrate and reason about features across the entire image is limited by the receptive field of convolutional layers. To achieve 3D spatially coherent reconstruction, we propose using two attention-based encoders, A_o and A_h , to merge the feature extracted by the feature extractors module. An attention score is computed for the two paired images by assessing the compatibility between a query and its corresponding key, producing two feature representations: one for the human $\varphi_h = A_h(\Phi_h^h, \Phi_f^h, \sigma_h(x_h))$ and another for the object $\varphi_o = A_o(\Phi_o^o, \Phi_f^o, \sigma_o(x_o))$. Notice that the pose features $\sigma_{\{h,o\}}$ obtained in the previous module are also concatenated. Each feature $\varphi_{\{h,o\}}$ integrates the information from its corresponding image $I_{\{h,o\}}$, combined with the global context of the input image I_f . This enables a more comprehensive understanding of the scene by using the multi-head self-attention layers of the transformer. As a result, the human feature φ_h contains detailed information from the human image, as well as contextual information of the scene from the input image. Similarly, the object feature φ_o integrates scene-level information from I_f .

Implicit function estimation: The implicit functions of the human f_h and object f_o are modeled with two separate multi-layer perceptrons (MLPs), which jointly estimate the occupancy values of X_h and X_o :

$$\hat{s} = \begin{cases} \hat{s}_h = f_h(\varphi_h, X_h), & \hat{s}_h \in \mathbb{R}, \\ \hat{s}_o = f_o(\varphi_o, X_o), & \hat{s}_o \in \mathbb{R} \end{cases} \quad (4)$$

where \hat{s} is the implicit representation of the final human-object shape, with \hat{s}_h representing the human component and \hat{s}_o representing the object component.

The neural implicit model is trained end-to-end with the following objective function $\mathcal{L} = \mathcal{L}_h + \mathcal{L}_o$:

$$\mathcal{L}_h = \frac{1}{N_h} \sum_{j=1}^{N_h} \left| f_h(\varphi_h^j, X_h^j) - f_h^{gt}(\varphi_h^j, X_h^j) \right|^2 \quad (5)$$

where N_h is the number of points X_h and f_h^{gt} is the ground-truth implicit function for the human shape, and

$$\mathcal{L}_o = \frac{1}{N_o} \sum_{j=1}^{N_o} \left| f_o(\varphi_o^j, X_o^j) - f_o^{gt}(\varphi_o^j, X_o^j) \right|^2 \quad (6)$$

where N_o is the number of points X_o and f_o^{gt} is the ground-truth implicit function for the object shape.

Inference: During inference, an input RGB image I_f , containing both a human and an object, is first processed with semantic segmentation to generate separate masks for human M_p and object M_o . Human and object poses are also estimated from I_f . If the object partially occludes the human, the segmented human image I_p and the intersection mask M_i , are processed by the diffusion module. This results in a full-body image I_h from which the 2D normal map S_N is estimated. These outputs, along with the input image I_f , the object image I_o and the pose features $\sigma_{\{h,o\}}$ are then processed by the attention-based neural implicit model. This model estimates the occupancy \hat{s} of a set of random 3D points X of the 3D space. Finally, the 3D shape is obtained by extracting iso-surface $f = 0.5$ of the probability field \hat{s} at threshold 0.5 with the Marching Cubes algorithm [17].

4. Experiments

Datasets: Due to the lack of 3D human-object datasets, we introduce the dataset synHOR for training our model. synHOR is a synthetic dataset created using 526 3D human scans from Thuman 2.0 [44] and 27 3D object scans including all 20 objects from BEHAVE [2] and selected 7 from HODome [46]. We picked random pairs of human and object meshes, where the object was initialized with a random pose and optimized to be in contact with the human. We then simulated 6 random translations of the human-object pair within the FOV of a perspective camera placed at the origin, and rendered 180 views for each translation. Finally, we discard the images where the object is not in view. We train SCHOR with 500 subjects of synHOR. For quantitative evaluation, we use 99 images from synHOR. We test the generalization power of SCHOR by inferring the human-object shapes from real images taken from BEHAVE [2]. BEHAVE is a real-world dataset that captures interactions between 8 humans and 20 objects. Due to its real-world

setting, high-quality ground truth meshes are unavailable; therefore, we perform only a qualitative evaluation.

Implementation details. We use SAM [11] to segment the input image into object and human and create the masks M_p and M_i . CHORE [36] is applied for pose estimation of the human and object. Once the diffusion model generates the inpainted image, we segment the occluded body region with M_i and merge it into the partial human image I_p to obtain the full-body human image I_h . The 2D normal map is estimated from I_h using pix2pixHD [34] as in PIFuHD [29]. To train the attention-based neural implicit model, we sample two sets of $N = 200000$ points around the ground-truth object and human surfaces, using a mix of uniform and importance sampling with variances $\sigma = 0.06, 0.01, 0.035$. From these, we randomly select $N_h = N_o = 20000$ points to create the X_h and X_o subsets. These points are projected into the input images following the Kinect camera model from the BEHAVE dataset [2]. Both the diffusion and neural implicit models are trained on a single A100 GPU. See supplementary for additional details about implementation. **Metrics:** We follow the evaluation in SiTH [8] to compute 3D metrics point-to-surface distance (P2S), Chamfer distance (CD), normal consistency (Normal), Intersection over Union (IoU) and fScore [32] on the generated meshes. The metrics are computed between the combined 3D human-object ground truth and the estimated reconstruction, with the estimated shape aligned to the ground truth by rescaling and translating it to match the human centroid.

4.1. Ablation Study

Effectiveness of architecture configuration: We demonstrate the significant improvement achieved by using the architecture configuration explained in Sec. 3.2. 6 alternate configurations of the architecture of the attention-based neural implicit model of SCHOR are trained and tested:

- **Single MLP:** To prove the effectiveness of estimating an implicit representation for each human and object, this configuration uses a single MLP to estimate a single occupancy \hat{s} for both human and object.
- **Single Trans:** Use of only a single transformer encoder A to merge human, object and input image features. \hat{s}_h and \hat{s}_o are estimated from the merged feature using f_h and f_o .
- **Single All:** Combination of the previous two configurations with a single transformer encoder and a single MLP.
- **No Trans:** The embeddings $\phi_{\{h,o,f\}}$ from the feature extractors are simply concatenated without applying the transformer encoders, highlighting the benefit of using self-attention. \hat{s}_h and \hat{s}_o are estimated.
- **Concat Trans:** Instead of extracting features directly from I_f , this configuration concatenates I_f with both I_h and I_o . ϕ_f is not extracted. ϕ_o and ϕ_h are merged with a transformer encoder before estimating \hat{s}_h and \hat{s}_o .
- **Concat No Trans:** Similar to **Concat Trans**, but ϕ_o and

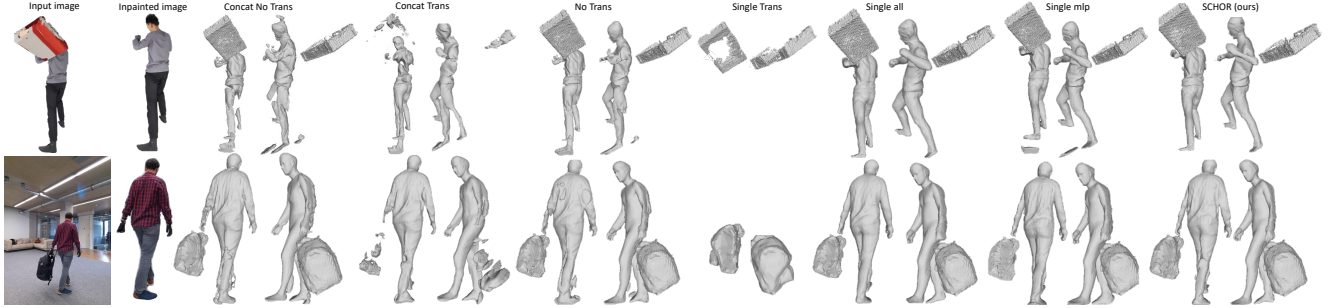


Figure 4. Qualitative results showing the effect of using different configurations of the attention-based neural implicit model. Front and side views are shown from synHOR in the top row, from BEHAVE [2] in the bottom.

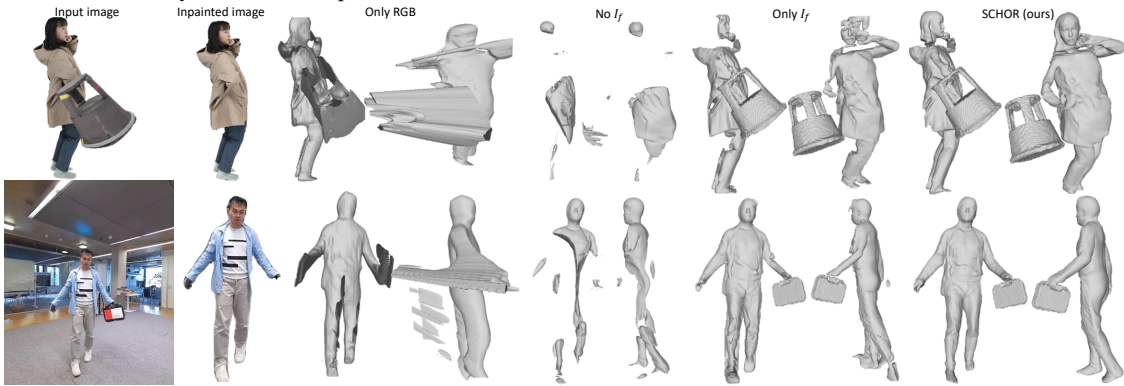


Figure 5. Qualitative results showing the effect of using different combinations of input data. Front and side views are shown from synHOR in the top row, and on BEHAVE [2] in the bottom row.

ϕ_h are processed separately by f_h and f_o respectively.

Both quantitative (Tab. 1) and qualitative (Fig. 4) results prove that the SCHOR’s architecture outperforms the other configurations. Specifically, replacing two MLPs with one (**Single MLP**) reduces reconstruction accuracy and detail, as seen in the hand of the BEHAVE model. If two MLPs process the same feature obtained by merging all the features with a single transformer (**Single Trans**), human-specific information is lost, resulting in an incomplete human reconstruction. Using both a single MLP and a single transformer degrades quality, producing smoother surfaces than SCHOR. Omitting the transformer encoder altogether (**No Trans**) makes the network less robust and introduces noise in the reconstruction. Finally, concatenating the input image I_f directly with I_o and I_h , significantly reduces quality compared to SCHOR, both when a transformer is used to merge human-object features (**Concat Trans**) and when it is not (**Concat No Trans**), proving that extracting features directly from I_f improves performance.

Effect of different inputs: SCHOR uses multiple input data to reconstruct the human-object shape, including the RGB image I_f , full-body human image I_h , 2D surface normal S_N , segmented object I_o and human-object pose. In this ablation study, we show the advantages of combining all these inputs. We adapt SCHOR architecture to process different combinations of the input data. In each configura-

Methods	synHOR				
	P2S ↓	CD ↓	IoU ↑	Normal ↑	f-Score ↑
Concat No Trans	25.59	30.38	.8246	.7324	29.66
Concat Trans	48.75	84.18	.4057	.5440	9.459
No Trans	22.90	24.66	.8447	.7683	33.97
Single All	15.05	18.12	.8752	.8248	47.71
Single Trans	52.78	101.1	.2284	.5406	7.103
Single MLP	17.57	24.70	.8267	.7986	43.98
SCHOR (ours)	14.23	17.15	.8902	.8241	48.84

Table 1. Quantitative results on synHOR dataset obtained by modifying the architecture of the network.

tion, two MLPs are still used to estimate \hat{s}_h and \hat{s}_o .

- **No S_N :** Same configuration as SCHOR but without 2D normal map S_N concatenated to I_h .
- **No $\sigma_{\{h,o\}}$:** Same configuration as SCHOR but without processing the human-object pose features $\sigma_{\{h,o\}}$.
- **Only RGB:** Same configuration as SCHOR excluding 2D normal map S_N and human-object pose features $\sigma_{\{h,o\}}$.
- **No I_f :** No input image I_f , so the image features $\Phi_f^{\{h,o\}}$ are not extracted. The human image feature Φ_h^h is merged with the object one Φ_o^o with a transformer encoder.
- **No I_o :** No object image I_o . The human image feature Φ_h^h is merged with the input image feature Φ_f^h using A_h .
- **No I_h :** No full-body human image I_h . The object feature Φ_o^o is merged with the input image feature Φ_f^o using A_o .
- **Only I_f :** Only the input image I_f is processed. No transformer is applied.

The benefit of incorporating all input data types is demon-

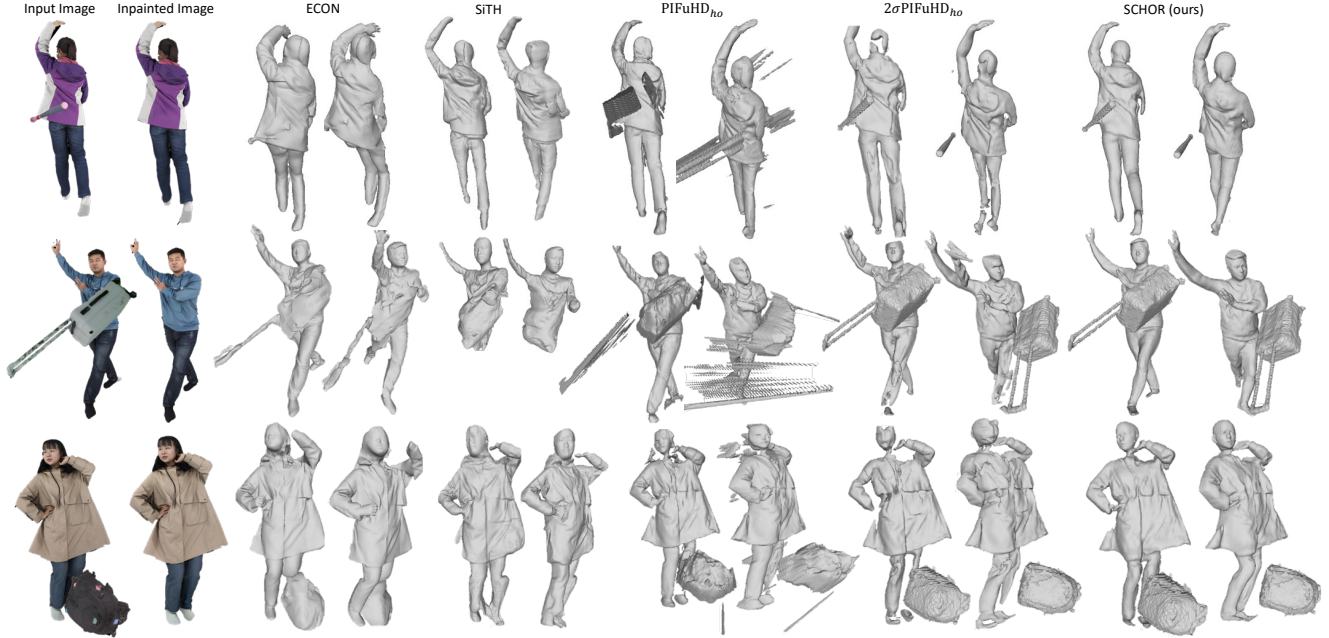


Figure 6. Visual comparisons from synHOR dataset with approaches that aim to reconstruct 3D humans as well as with baselines designed for fair comparisons. Front and side views are shown.

Methods	synHOR				
	P2S ↓	CD ↓	IoU ↑	Normal ↑	f-Score ↑
Only RGB	47.86	78.25	.4472	.5962	11.33
No $\sigma_{h,o}$	44.14	71.72	.5064	.6175	12.85
No S_N	14.24	17.12	.8661	.8024	41.46
Only I_f	28.82	36.83	.6966	.7196	25.62
No I_f	45.80	100.0	.3473	.5284	5.76
No I_h	53.24	108.4	.2239	.5374	7.66
No I_o	51.77	91.32	.3516	.5535	8.88
SCHOR (ours)	14.23	17.15	.8902	.8241	48.84

Table 2. Quantitative results on synHOR dataset obtained with different combinations of input data.

Methods	synHOR				
	P2S ↓	CD ↓	IoU ↑	Normal ↑	f-Score ↑
PIFuHD	33.75	67.59	.4555	.6595	18.07
ECON	36.48	79.39	.3952	.6547	14.57
SiTH	31.88	68.88	.3371	.6521	14.33
PIFuHD _{ho}	43.50	91.97	.3917	.5661	11.00
σ PIFuHD _{ho}	31.66	50.78	.4228	.7090	20.59
2PIFuHD _{ho}	48.29	80.09	.3482	.5347	10.79
2 σ PIFuHD _{ho}	28.82	36.83	.6966	.7196	25.62
2 σ PIFuHD _{ho} ^{sep}	25.83	33.20	.8176	.7204	29.17
2 σ PIFuHD _{ho} ^{all}	23.87	26.53	.8172	.7601	32.72
SCHOR (ours)	14.23	17.15	.8902	.8241	48.84

Table 3. Quantitative comparisons on synHOR dataset between SCHOR and related works that aim to reconstruct high-quality 3D shape in the bottom part. Results from comparisons with baselines created from PIFuHD [29] for fair comparisons are also presented.

strated by the superior quantitative results in Tab. 2. This is further supported by the visual results in Fig. 5, where more realistic and accurate human-object shapes are obtained with SCHOR. When the input RGB image is omitted (No I_f), the model lacks global scene understanding, resulting in severe artifacts. Likewise, if human and object images are not used (Only I_f), the network lacks local in-

formation about them. **Only RGB** shows the importance of using both normal maps and pose features to reproduce realistic details and ensure 3D spatial coherency in the reconstruction. Additional ablations are in the supplementary.

4.2. Comparisons

Our goal is to demonstrate that SCHOR can jointly reconstruct 3D human-object shapes from single-view images, producing realistic, detailed, and spatially coherent outputs. To the best of our knowledge, SCHOR is the first framework to address this task since related works either focus solely on realistic human reconstruction or model human-object interactions using template-based shapes, limiting detail and reducing the realism of reconstructions. We compare SCHOR with approaches of both categories.

Realistic human reconstruction methods: We evaluate SCHOR against methods designed for high-quality human shape reconstruction from single images using neural implicit models (PIFuHD [29], ECON [41], SiTH [8]). To demonstrate that these works cannot jointly reconstruct human and object shapes, we use the RGB image I_f as input. For a fair comparison, we retrain PIFuHD on synHOR (PIFuHD_{ho}) and introduce several baseline models based on the PIFuHD architecture to showcase SCHOR’s superiority in joint human-object reconstruction. We first use two MLPs instead of one to estimate an implicit representation of both human and object (2PIFuHD_{ho}). Since PIFuHD does not rely on 3D spatial information, we repeat the previous experiments by concatenating the human-object pose feature σ to the extracted features (indicated with the prefix σ). Then, features are extracted from only the segmented

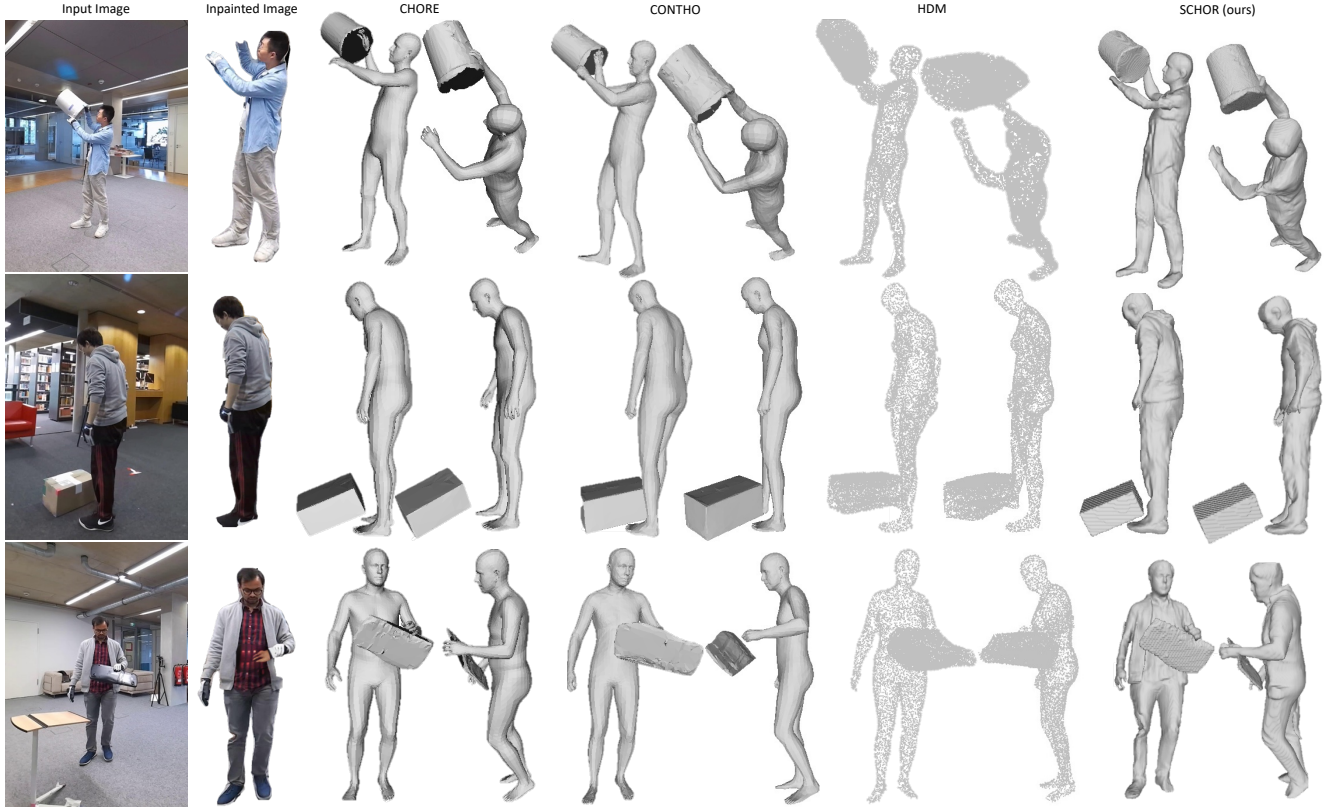


Figure 7. Qualitative evaluations against methods which aim to model the human-object interaction with examples from BEHAVE dataset [2]. Note that HDM generates point clouds rather than meshes. Front and side views are shown.

human and object images ($2\sigma\text{PIFuHD}_{\text{ho}}^{\text{sep}}$) and finally, the images (I_f, I_h, I_o) are concatenated together as input before feature extraction ($2\sigma\text{PIFuHD}_{\text{ho}}^{\text{all}}$).

As shown in Tab. 3, SCHOR achieves the best quantitative results and, as seen in Fig. 6, is the only approach able to reconstruct realistic, spatially coherent human-object shapes without noise. Human-focused approaches (ECON, SiTH, PIFuHD) struggle with object reconstruction, impacting human shape quality as well. Retraining these models with the synHOR dataset ($\text{PIFuHD}_{\text{ho}}$) and even adding two MLPs and pose parameters ($2\sigma\text{PIFuHD}_{\text{ho}}$) is insufficient to achieve the realism of SCHOR, which outperforms all approaches significantly.

Parametric human-object reconstruction methods: We also compare SCHOR against state-of-the-art parametric-model based methods for human-object reconstruction from a single image, mainly CHORE [36], CONTHO [20] and HDM [38]. As shown in Fig. 7, SCHOR is the only method that reconstructs realistic clothed human-object shapes. Related works use a parametric-based representation of humans, which lacks detail and significantly reduces realism. These parametric approaches are designed to model human-object interactions explicitly. Our results show that despite not being trained on an explicit human-object interaction dataset, SCHOR implicitly reconstructs human-object interactions due to its spatial awareness. Note that we do not

quantitatively evaluate parametric methods as the realism of their shapes is much lower than non-parametric shapes.

See supplementary for additional comparison results.

Limitations and Future work: Realistic clothed human-object reconstruction is an extremely challenging problem. In this work, we do not explicitly model human-object interactions, which can be less accurate than related works that focus on this. We specifically address the case where the human is occluded by an object, and not vice-versa. Finally, SCHOR leverages object poses estimated from known object templates, limiting its generalization to unseen objects. In future work, we will address these limitations by proposing a method that can handle occluded objects and explicitly model human-object interactions. We will also aim to retrieve textures of the clothed human-object reconstruction.

5. Conclusion

We presented SCHOR, the first novel method that can jointly reconstruct realistic clothed humans and objects from a human-object scene image. SCHOR combines the power of attention-based neural implicit learning with a generative diffusion model and human-object pose conditioning to produce detailed, spatially coherent human-object 3D shapes. Extensive ablations on various network architecture components of SCHOR demonstrate the effec-

tiveness of the proposed approach. Our experiments show that our method generalizes well to a real world dataset on which it was not trained and outperforms the state-of-the-art methods in reconstructing realistic human-object scenes.

Joint Reconstruction of Spatially-Coherent and Realistic Clothed Humans and Objects from a Single Image

Supplementary Material

6. Overview

In the following sections of the supplementary material we present:

- Additional details about the implementation of SCHOR (Sec. 7);
- A table containing a list of symbol used in the main paper is presented in Sec. 8
- Additional ablation studies to demonstrate the effectiveness of the proposed framework (Sec. 9);
- Additional results of SCHOR and related works on both synHOR and BEHAVE [2] datasets (Sec. 10);
- A more detailed discussion about results, limitations and future works (Sec. 11);

7. Implementation details

7.1. Diffusion model

Inspired by SitH [8], our image-conditioned latent diffusion model [26] used to generate missing body regions as described in Sec. 3.1, is trained by fine-tuning the diffusion U-Net’s [26] weights. These weights are initialized using the Zero-1-to-3 [18] model, combined with a trainable ControlNet [48] model, following the default network setups with input channel adjustment. The ControlNet input is a 1 channel mask and the diffusion U-Net input is a 3-channel RGB image of size 512 x 512. We train the models with a batch size of 6 images on a single A100 NVIDIA GPU, with a learning rate of 4×10^{-6} and adopting a constant warmup scheduling. The ControlNet model’s conditioning scale is fixed at 1.0. We use classifier-free guidance in our training, involving a dropout rate of 0.05 for the image-conditioning. During inference, a classifier-free guidance scale of 2.5 is applied to generate the output images.

7.2. Attention-based neural implicit model

We detail the implementation of our attention-based neural implicit model described in Sec. 3.2. For each input image of size 2048x1536, we take a crop around the human-object bounding box center and resize it to 512px for the network. Following PIFu [28], we use a four-stack Hourglass network that yields a 256-dimensional feature map for querying pixel-aligned features. A standard multi-head transformer-style architecture is applied for the two attention-based encoders A_h and A_o , as shown in Fig. 3. Given three vectors query $Q = M_q\phi$, key $K = M_k\phi$ and value $V = M_v\phi$ as the embedding of the original feature Φ and parameterized by matrices M_q , M_k and M_v , an at-

Symbol	Definition
I_f	Input RGB image
I_o	Segmented object image
I_p	Segmented partial human image
I_h	Generated full-body human image
S_N	Estimated 2D normal map
$\sigma_{\{h,o\}}$	Human and object pose features
M_i	Mask of occluded human body regions
M_s	Mask of SMPL human model
M_p	Mask of partial human
ε	Variational Auto Encoder
ϵ_θ	Diffusion U-Net
\mathcal{D}	Diffusion decoder
f_θ	Iterative denoising process of ϵ_θ
$\phi_{\{h,o,f\}}$	Feature extracted with stacked hourglass networks from I_h , I_o and I_f
$X_{\{h,o\}}$	3D points sampled in human and object 3D ground-truth meshes
$\Phi_{\{h,o,f\}}^{\{h,o\}}$	Pixel-aligned human and object features by projecting X_h and X_o in $\phi_{\{h,o,f\}}$
$A_{\{h,o\}}$	Transformer encoders to merge human and object features with image features
$\varphi_{\{h,o\}}$	Merged human and object features output of $A_{\{h,o\}}$
$f_{\{h,o\}}$	Implicit functions (MLPs)
$\hat{s}_{\{h,o\}}$	Human and object implicit representations

Table 4. List of notations used in the main paper.

tion score is computed for each input feature $\Phi_{\{h,f\}}^h$ for A_h and $\Phi_{\{o,f\}}^o$ for A_o based on the compatibility of a query with a corresponding key:

$$Attention(Q, K, V) = softmax\left(\frac{QK^T}{\sqrt{d_k}}\right)V \quad (7)$$

where d_k is the common dimension of K , Q and V . Multiple heads are used to compute features for the human and object:

$$MultiHead(Q, K, V) = concat(H_1, \dots, H_h)W^o \quad (8)$$

$$H_i = Attention(QW_i^q, KW_i^k, VW_i^v)$$

where QW_i^q , KW_i^k , VW_i^v are the parameters of Q , K and V , and W^o the parameters of the final projection. The final feature is computed as the mean of the processed features. with each merged feature $\varphi_{\{h,o\}}$ containing local information from the human or object image along with global scene information from the input image. Finally, to estimate the neural implicit representations, each decoder f_h , f_o is an MLP with the number of neurons (259, 1024, 512, 256, 128, 1) and skip connections at 2nd, 3rd and 4th layers. We train the network end-to-end using Adam optimizer with a learning rate of $1e-4$ and batch size 4.

8. Notations

To facilitate the understanding of the main paper, Tab. 4 presents a list of the notations used in the paper.

9. Additional ablation studies

9.1. Effect of different inputs

Fig. 5 of the main paper shows examples of human-object shapes reconstructed using different combinations of input. Additional results from the configurations analyzed in the second ablation study of Sec. 4.1 and not included in Fig. 5 are shown in Fig. 8. The highest quality human-object shapes are obtained using SCHOR, confirming what was proved in Sec. 4.1. Smoother shapes are reconstructed when normal maps are excluded (No S_N) while omitting pose features (No $\sigma_{h,o}$) introduces depth ambiguity. Excluding the full-body human input (No I_h) or the object input (No I_o) prevents the network from reconstructing the human or object, respectively.

9.2. Training configurations

Methods	synHOR				
	P2S ↓	CD ↓	IoU ↑	Normal ↑	f-Score ↑
Sep _{no}	23.36	27.22	.8337	.7523	34.38
Sep	47.69	81.93	.4564	.5868	10.27
SCHOR (ours)	14.23	17.15	.8902	.8241	48.84

Table 5. Quantitative results obtained with different training configurations of SCHOR.

The proposed attention-based neural implicit model is trained end-to-end to enable better joint reasoning about the human-object scene. This section presents results obtained by modifying SCHOR’s training configuration:

- **Sep_{no}**: Two separate networks are trained. One reconstructs the human shape using the full-body human image generated by the inpainting diffusion model and the relative human pose feature. The other reconstructs the

object shape using the object image and pose feature. No transformer encoder is used.

- **Sep**: Similar to Sep_{no}, two networks are trained separately to estimate the human and object implicit representations. However, in this configuration, the input RGB image is also considered. Each network extracts features from the input RGB image and merges them with either the full-body human or object features using transformer encoders.

As demonstrated by the quantitative evaluation in Tab. 5 and the qualitative results (Fig. 9), training the attention-based neural implicit model end-to-end significantly improves performance. Both Sep and Sep_{no} training configurations result in less accurate human-object reconstructions.

9.3. Inpainting module

Methods	synHOR				
	P2S ↓	CD ↓	IoU ↑	Normal ↑	f-Score ↑
No inpainting	19.19	22.24	.8679	.8080	40.77
MAT	15.39	18.94	.8841	.8132	46.44
Normal	15.18	17.70	.8860	.8163	47.02
Both	14.91	18.49	.8859	.8160	48.26
SCHOR (ours)	14.23	17.15	.8902	.8241	48.84

Table 6. Quantitative evaluation of changing the diffusion module of SCHOR. The human-object shapes reconstructed with the attention-based neural implicit module of SCHOR are used for evaluation.

In scenes containing both humans and objects, the object often occlude parts of the human body. When only partial regions of the body are visible, the network fails to reconstruct the occluded regions. This limitation is shown in Fig. 10, where SCHOR is applied without the inpainting module to generate a full-body human image. Instead, the partial human image is directly input into the attention-based neural implicit model, which fails to reconstruct these occluded regions, producing holes in the human shapes. Inpainting the

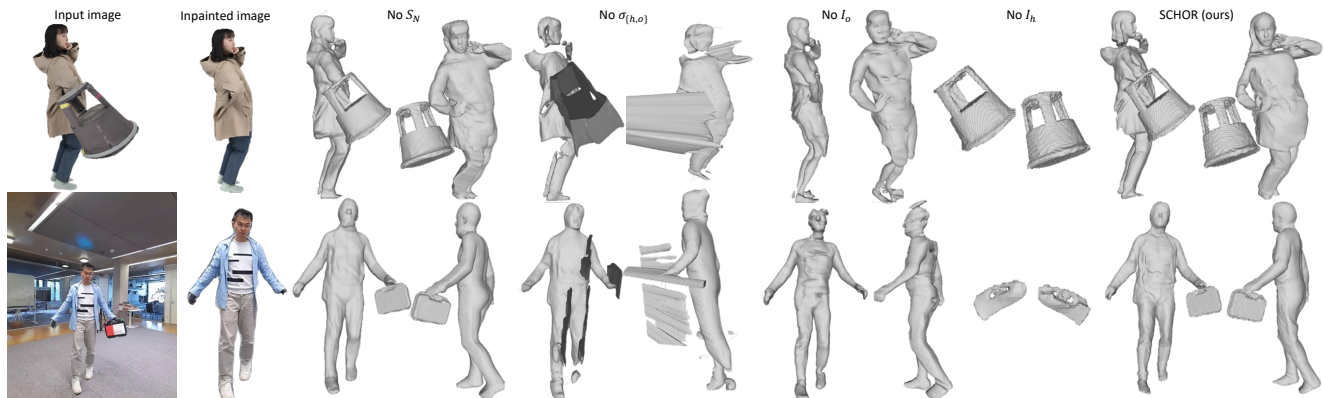


Figure 8. Qualitative results showing the effect of using different configurations of the attention-based neural implicit model with methods that have not been shown in Fig. 5 of the main paper. Front and side views are shown from synHOR in the top row, from BEHAVE [2] in the bottom.

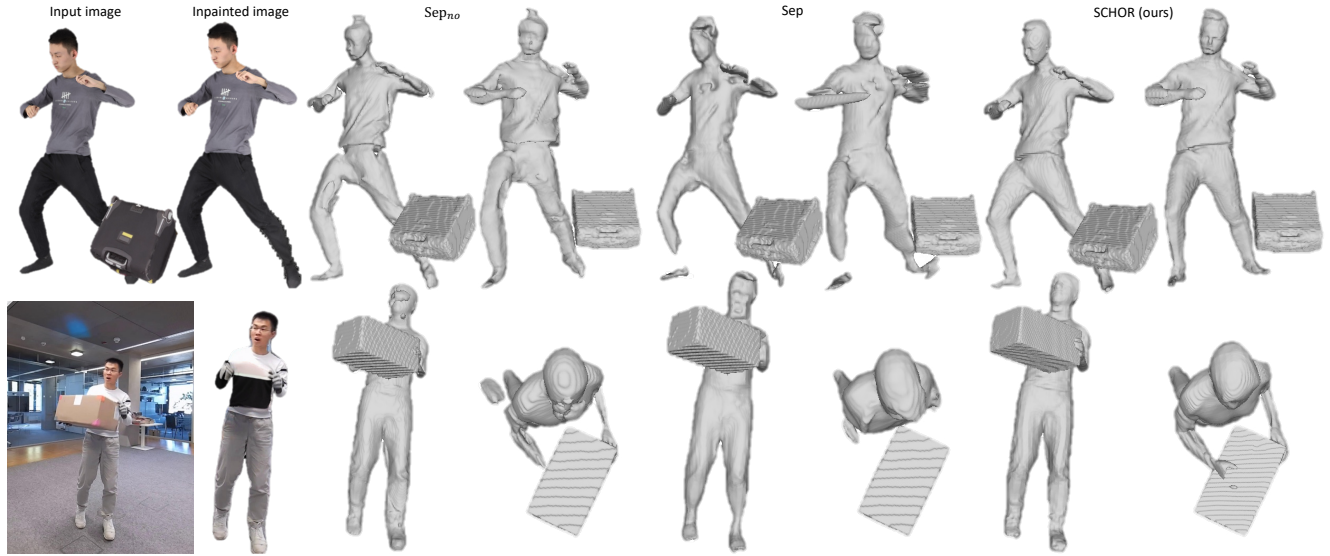


Figure 9. Examples of results obtained with different training configurations of SCHOR. Front and side views are shown from synHOR in the top row, from BEHAVE [2] in the bottom.

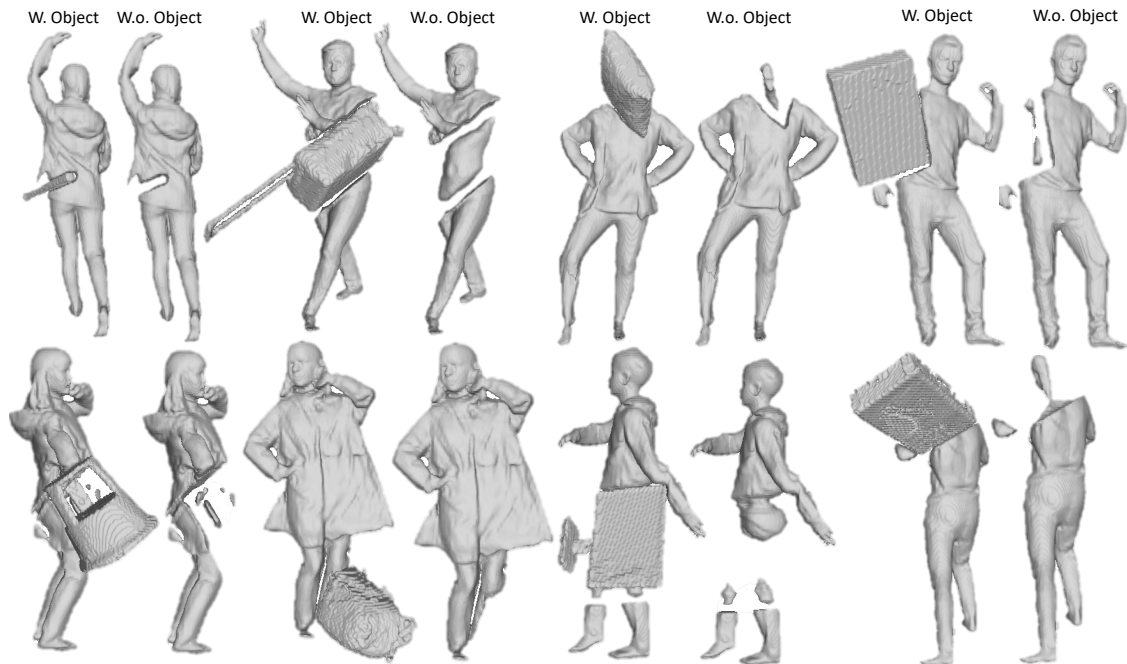


Figure 10. Effect of not applying the inpainting module of SCHOR before estimating the implicit representation. The same examples used in the paper are illustrated with (w.) and without (w.o) the object.

missing body regions in the input image is crucial to reconstruct realistic human-object shapes.

SCHOR addresses the challenge of human occlusion by leveraging the generative capability of diffusion models to inpaint the occluded body regions. A fine-tuning strategy is adopted to optimize the cross-attention layers of a pre-trained diffusion model, conditioning it on the mask of the body regions requiring inpainting. In this section, we ex-

plore different solutions for inpainting, including MAT [15], a transformer-based model for large hole inpainting, conditioning the diffusion model with the SMPL [27] normal map (Normal), and conditioning with both the mask and the normal map (Both). The effect of using these approaches for the inpainting module of SCHOR is quantitatively evaluated by estimating the implicit representation of human-object shapes using their generated full-body human im-



Figure 11. Visual comparisons of inpainted images generated using different inpainting approaches.

age (Tab. 6). Examples of human-object reconstructions using these methods for inpainting are shown in Fig. 12 while Fig. 11 illustrates the input images shown in the paper and generated using the discussed inpainting methods.

As expected, the worst results occur when no inpainting is applied (No inpainting). MAT struggles to produce realistic body regions in the RGB images, propagating noise into the final reconstruction. Conditioning the diffusion model with both the SMPL normal map and the mask also degrades performance. The best results are achieved when either the SMPL normal or the mask of the occluded regions is processed using ControlNet. In particular, processing only the mask proves more robust, as seen in the top-left example of Fig. 11 and in the reconstructed human-object shape in the top row of Fig. 12, where unnatural black regions in the full-body human image generated with Normal configuration caused gaps in the reconstructed shape.

Note that we do not quantitatively evaluate the generated

images against ground truth, since the main goal of SCHOR is 3D reconstruction rather than inpainting.

10. Additional visual comparisons

In this section, we present additional visual results of human-object shapes reconstructed using SCHOR, as well as comparisons with related methods that aim to reconstruct high-quality 3D humans (PIFuHD [29], ECON [41], SiTH [8]) and the baseline models introduced in Sec. 4.2 of the main paper. Specifically, Fig. 13 presents results of the methods not included in Fig. 6 of the main paper on synHOR dataset, while Fig. 14 illustrates reconstructed human-object shapes on the BEHAVE [2] dataset that were omitted from Fig. 7. Fig. 15 and Fig. 16 show new examples of reconstructed shapes using the considered methods on synHOR and BEHAVE dataset, respectively. Across all the presented figures, our approach reconstructs the most realistic human-object shapes with the fewest artefacts com-



Figure 12. Human-object shapes reconstructed by changing the diffusion module of SCHOR. Front view with and without the object and side views without the object are shown from synHOR in the top row, from BEHAVE [2] in the bottom.

pared to related works. While human-focused reconstruction approaches achieve higher detail in human shapes, they cannot reconstruct objects, failing to achieve our goal of joint human-object reconstruction. Even retraining PIFuHD on synHOR (σ PIFuHD_{ho}), incorporating pose features (σ PIFuHD_{ho}), or using two MLPs (2σ PIFuHD_{ho}), does not sufficiently improve results, with severe depth ambiguities in the reconstructed objects. The proposed baselines that leverage pose features along with two MLPs (2σ PIFuHD_{ho}, 2σ PIFuHD_{ho}^{all}, 2σ PIFuHD_{ho}^{sep}) can reconstruct objects but are significantly more prone to noise and artifacts compared to SCHOR. The attention-based neural implicit model introduced by SCHOR ensures the joint reconstruction of spatially coherent and realistic human-object shapes from single images, outperforming all related approaches.

11. Discussion

Existing works [8, 29, 41] for high-quality human reconstruction are not designed to reconstruct objects. Consequently, when these methods are applied to real images containing both humans and objects, they behave differently in accordance with their network design, as illustrated in Fig. 14. For instance, if these methods are conditioned on the SMPL model [8, 41], the object is not reconstructed unless it is very close to the human. In such cases, these methods misinterpret the object as part of the clothing, merging it with the human mesh and resulting in a lack of 3D spatial coherence. Similarly, methods that integrate normals [29] to reconstruct human shapes struggle to distinguish between clothing and objects, treating them as a single entity. One potential solution is to crop the object out of the image and reconstruct only the human with the above methods. However, this requires reconstructing the object separately,



Figure 13. Visual comparisons from synHOR with related works not shown in Fig. 6 of the main paper. Front and side views are shown.

without considering its spatial relation with the human. In contrast, our approach is explicitly designed to jointly reason about humans and objects, distinguishing them as two distinct yet connected entities and reconstructing both in a spatially coherent manner.

We also highlight the importance of extracting features from each considered input and merging them using transformer encoders. This allows a better understanding of the global scene, ensuring 3D spatial coherence. In addition, learning local information about humans and objects allows our method to reproduce fine details in the human-object shapes.

Despite its strengths, our approach is prone to certain limitations. First, the reconstruction quality of smaller body parts, such as fingers and hair, can be improved. This refinement is essential for explicitly modelling human-object interactions and will be addressed in future work. Furthermore, the reconstruction quality of unseen regions in the full-body human image, such as the sides and back, is limited.

Another limitation arises from estimating the object pose features from known templates. This restricts the method’s ability to generalize to objects without predefined templates. Future work will explore strategies to estimate pose parameters without using templates.

Our method relies on state-of-the-art works for human-object pose and normal map estimation. As a result, if these estimations are noisy, the noise propagates through the pipeline, causing artifacts in the reconstructed human shape. Note that all the quantitative results on synHOR use ground-truth SMPL-H models and occlusion masks, while 2D normal maps are generated with pix2pixHD [34] from the inpainted images.

Finally, a key direction for future work involves estimating the appearance of clothed human-object reconstructions to further enhance realism.



Figure 14. Visual comparisons from BEHAVE [2] dataset with approaches that aim to reconstruct 3D humans as well as with baselines designed for fair comparisons. The same examples shown in Fig. 7 are illustrated. Front and side views are shown.



Figure 15. Additional visual results from synHOR. Examples obtained with methods that aim to reconstruct 3D humans as well as with the baselines considered in the main paper are shown. Front and side views are shown.



Figure 16. Additional visual results from BEHAVE [2]. Examples obtained with methods that aim to reconstruct 3D humans as well as with the baselines considered in the main paper are shown. Front and side views are shown.

References

- [1] Mohammad Samiul Arshad and William J Beksi. List: Learning implicitly from spatial transformers for single-view 3d reconstruction. In *Proceedings of the IEEE/CVF International Conference on Computer Vision*, pages 9321–9330, 2023. 1, 2
- [2] Bharat Lal Bhatnagar, Xianghui Xie, Ilya A Petrov, Cristian Sminchisescu, Christian Theobalt, and Gerard Pons-Moll. Behave: Dataset and method for tracking human object interactions. In *Proceedings of the IEEE/CVF Conference on Computer Vision and Pattern Recognition*, pages 15935–15946, 2022. 2, 5, 6, 8, 1, 3, 4, 7, 9
- [3] Rongshan Chen, Yuancheng Yang, and Chao Tong. G2ifu: Graph-based implicit function for single-view 3d reconstruction. *Engineering Applications of Artificial Intelligence*, 124: 106493, 2023. 1, 2
- [4] Yixin Chen, Siyuan Huang, Tao Yuan, Siyuan Qi, Yixin Zhu, and Song-Chun Zhu. Holistic++ scene understanding: Single-view 3d holistic scene parsing and human pose estimation with human-object interaction and physical commonsense. In *Proceedings of the IEEE/CVF International Conference on Computer Vision*, pages 8648–8657, 2019. 2
- [5] Zhiqin Chen and Hao Zhang. Learning implicit fields for generative shape modeling. In *Proceedings of the IEEE/CVF conference on computer vision and pattern recognition*, pages 5939–5948, 2019. 2
- [6] George Fahim, Khalid Amin, and Sameh Zarif. Enhancing single-view 3d mesh reconstruction with the aid of implicit surface learning. *Image and Vision Computing*, 119:104377, 2022. 1, 2
- [7] Tong He, John Collomosse, Hailin Jin, and Stefano Soatto. Geo-pifu: Geometry and pixel aligned implicit functions for single-view human reconstruction. *Advances in Neural Information Processing Systems*, 33:9276–9287, 2020. 1, 2
- [8] I Ho, Jie Song, Otmar Hilliges, et al. Sith: Single-view textured human reconstruction with image-conditioned diffusion. In *Proceedings of the IEEE/CVF Conference on Computer Vision and Pattern Recognition*, pages 538–549, 2024. 1, 2, 3, 5, 7, 4
- [9] Yuheng Jiang, Suyi Jiang, Guoxing Sun, Zhuo Su, Kaiwen Guo, Minye Wu, Jingyi Yu, and Lan Xu. Neuralhofusion: Neural volumetric rendering under human-object interactions. In *Proceedings of the IEEE/CVF Conference on Computer Vision and Pattern Recognition*, pages 6155–6165, 2022. 2
- [10] Yuheng Jiang, Kaixin Yao, Zhuo Su, Zhehao Shen, Haimin Luo, and Lan Xu. Instant-nvr: Instant neural volumetric rendering for human-object interactions from monocular rgbd stream. In *Proceedings of the IEEE/CVF Conference on Computer Vision and Pattern Recognition*, pages 595–605, 2023. 2
- [11] Alexander Kirillov, Eric Mintun, Nikhila Ravi, Hanzi Mao, Chloe Rolland, Laura Gustafson, Tete Xiao, Spencer Whitehead, Alexander C Berg, Wan-Yen Lo, et al. Segment anything. In *Proceedings of the IEEE/CVF International Conference on Computer Vision*, pages 4015–4026, 2023. 5
- [12] Nikos Kolotouros, Thiemo Alldieck, Enric Corona, Eduard Gabriel Bazavan, and Cristian Sminchisescu. Instant 3d human avatar generation using image diffusion models. *arXiv preprint arXiv:2406.07516*, 2024. 2
- [13] Nupur Kumari, Bingliang Zhang, Richard Zhang, Eli Shechtman, and Jun-Yan Zhu. Multi-concept customization of text-to-image diffusion. In *Proceedings of the IEEE/CVF Conference on Computer Vision and Pattern Recognition*, pages 1931–1941, 2023. 3
- [14] Manyi Li and Hao Zhang. D2im-net: Learning detail disentangled implicit fields from single images. In *Proceedings of the IEEE/CVF Conference on Computer Vision and Pattern Recognition*, pages 10246–10255, 2021. 2
- [15] Wenbo Li, Zhe Lin, Kun Zhou, Lu Qi, Yi Wang, and Jiaya Jia. Mat: Mask-aware transformer for large hole image inpainting. In *Proceedings of the IEEE/CVF Conference on Computer Vision and Pattern Recognition*, 2022. 3
- [16] Shichen Liu, Shunsuke Saito, Weikai Chen, and Hao Li. Learning to infer implicit surfaces without 3d supervision. *Advances in Neural Information Processing Systems*, 32, 2019. 2
- [17] William E Lorensen and Harvey E Cline. Marching cubes: A high resolution 3d surface construction algorithm. *ACM siggraph computer graphics*, 21(4):163–169, 1987. 5
- [18] Camillo Lugaresi, Jiuqiang Tang, Hadon Nash, Chris McClanahan, Esha Uboweja, Michael Hays, Fan Zhang, Chuo-Ling Chang, Ming Yong, Juhyun Lee, et al. Mediapipe: A framework for perceiving and processing reality. In *Third workshop on computer vision for AR/VR at IEEE computer vision and pattern recognition (CVPR)*, 2019. 1
- [19] Lars Mescheder, Michael Oechsle, Michael Niemeyer, Sebastian Nowozin, and Andreas Geiger. Occupancy networks: Learning 3d reconstruction in function space. In *Proceedings of the IEEE/CVF conference on computer vision and pattern recognition*, pages 4460–4470, 2019. 2
- [20] Hyeongjin Nam, Daniel Sungho Jung, Gyeongsik Moon, and Kyoung Mu Lee. Joint reconstruction of 3d human and object via contact-based refinement transformer. In *Proceedings of the IEEE/CVF Conference on Computer Vision and Pattern Recognition*, 2024. 1, 2, 4, 8
- [21] Jeong Joon Park, Peter Florence, Julian Straub, Richard Newcombe, and Steven Lovegrove. DeepSDF: Learning continuous signed distance functions for shape representation. In *Proceedings of the IEEE/CVF conference on computer vision and pattern recognition*, pages 165–174, 2019. 2
- [22] Marco Pesavento, Marco Volino, , and Adrian Hilton. Super-resolution 3d human shape from a single low-resolution image. In *ECCV*, 2022. 1, 2, 4
- [23] Marco Pesavento, Yuanlu Xu, Nikolaos Sarafianos, Robert Maier, Ziyang Wang, Chun-Han Yao, Marco Volino, Edmond Boyer, Adrian Hilton, and Tony Tung. Anim: Accurate neural implicit model for human reconstruction from a single rgb-d image. In *Proceedings of the IEEE/CVF Conference on Computer Vision and Pattern Recognition*, pages 5448–5458, 2024. 2
- [24] Marco Pesavento, Marco Volino, and Adrian Hilton. Cosmu: Complete 3d human shape from monocular unconstrained

- images. In *European Conference on Computer Vision*, pages 201–219. Springer, 2025. 2
- [25] Aditya Ramesh, Prafulla Dhariwal, Alex Nichol, Casey Chu, and Mark Chen. Hierarchical text-conditional image generation with clip latents. *arXiv preprint arXiv:2204.06125*, 1(2):3, 2022. 3
- [26] Robin Rombach, Andreas Blattmann, Dominik Lorenz, Patrick Esser, and Björn Ommer. High-resolution image synthesis with latent diffusion models. In *Proceedings of the IEEE/CVF conference on computer vision and pattern recognition*, pages 10684–10695, 2022. 3, 1
- [27] Javier Romero, Dimitrios Tzionas, and Michael J. Black. Embodied hands: Modeling and capturing hands and bodies together. *ACM Transactions on Graphics, (Proc. SIGGRAPH Asia)*, 36(6), 2017. 3
- [28] Shunsuke Saito, Zeng Huang, Ryota Natsume, Shigeo Morishima, Angjoo Kanazawa, and Hao Li. Pifu: Pixel-aligned implicit function for high-resolution clothed human digitization. In *Proceedings of the IEEE/CVF International Conference on Computer Vision*, pages 2304–2314, 2019. 2, 4, 1
- [29] Shunsuke Saito, Tomas Simon, Jason Saragih, and Hanbyul Joo. Pifuhd: Multi-level pixel-aligned implicit function for high-resolution 3d human digitization. In *Proceedings of the IEEE/CVF Conference on Computer Vision and Pattern Recognition*, pages 84–93, 2020. 1, 2, 4, 5, 7
- [30] Akash Sengupta, Thiemo Alldieck, Nikos Kolotouros, Enric Corona, Andrei Zanfir, and Cristian Sminchisescu. Diffhuman: Probabilistic photorealistic 3d reconstruction of humans. In *Proceedings of the IEEE/CVF Conference on Computer Vision and Pattern Recognition*, pages 1439–1449, 2024. 2
- [31] Guoxing Sun, Xin Chen, Yizhang Chen, Anqi Pang, Pei Lin, Yuheng Jiang, Lan Xu, Jingyi Yu, and Jingya Wang. Neural free-viewpoint performance rendering under complex human-object interactions. In *Proceedings of the 29th ACM International Conference on Multimedia*, pages 4651–4660, 2021. 2
- [32] Maxim Tatarchenko, Stephan R Richter, René Ranftl, Zhuwen Li, Vladlen Koltun, and Thomas Brox. What do single-view 3d reconstruction networks learn? In *Proceedings of the IEEE/CVF conference on computer vision and pattern recognition*, pages 3405–3414, 2019. 5
- [33] Jianyuan Wang, Huanqiang Xu, Xinrui Hu, and Biao Leng. Ifkd: Implicit field knowledge distillation for single view reconstruction. *Mathematical Biosciences and Engineering*, 20(8):13864–13880, 2023. 1, 2
- [34] Ting-Chun Wang, Ming-Yu Liu, Jun-Yan Zhu, Andrew Tao, Jan Kautz, and Bryan Catanzaro. High-resolution image synthesis and semantic manipulation with conditional gans. In *Proceedings of the IEEE conference on computer vision and pattern recognition*, pages 8798–8807, 2018. 5, 6
- [35] Xi Wang, Gen Li, Yen-Ling Kuo, Muhammed Kocabas, Emre Aksan, and Otmar Hilliges. Reconstructing action-conditioned human-object interactions using commonsense knowledge priors. In *2022 International Conference on 3D Vision (3DV)*, pages 353–362. IEEE, 2022. 2
- [36] Xianghui Xie, Bharat Lal Bhatnagar, and Gerard Pons-Moll. Chore: Contact, human and object reconstruction from a single rgb image. In *European Conference on Computer Vision*, pages 125–145. Springer, 2022. 1, 4, 5, 8
- [37] Xianghui Xie, Bharat Lal Bhatnagar, and Gerard Pons-Moll. Visibility aware human-object interaction tracking from single rgb camera. In *IEEE Conference on Computer Vision and Pattern Recognition (CVPR)*, 2023. 2, 4
- [38] Xianghui Xie, Bharat Lal Bhatnagar, Jan Eric Lenssen, and Gerard Pons-Moll. Template free reconstruction of human-object interaction with procedural interaction generation. In *IEEE Conference on Computer Vision and Pattern Recognition (CVPR)*, 2024. 1, 2, 8
- [39] Xianghui Xie, Jan Eric Lenssen, and Gerard Pons-Moll. Intertrack: Tracking human object interaction without object templates. *arXiv preprint arXiv:2408.13953*, 2024. 2
- [40] Yuliang Xiu, Jinlong Yang, Dimitrios Tzionas, and Michael J Black. Icon: Implicit clothed humans obtained from normals. In *2022 IEEE/CVF Conference on Computer Vision and Pattern Recognition (CVPR)*, pages 13286–13296. IEEE, 2022. 2
- [41] Yuliang Xiu, Jinlong Yang, Xu Cao, Dimitrios Tzionas, and Michael J Black. Econ: Explicit clothed humans optimized via normal integration. In *Proceedings of the IEEE/CVF Conference on Computer Vision and Pattern Recognition*, pages 512–523, 2023. 1, 2, 7, 4, 5
- [42] Qiangeng Xu, Weiyue Wang, Duygu Ceylan, Radomir Mech, and Ulrich Neumann. Disn: Deep implicit surface network for high-quality single-view 3d reconstruction. *Advances in neural information processing systems*, 32, 2019. 2
- [43] Xiang Xu, Hanbyul Joo, Greg Mori, and Manolis Savva. D3d-hoi: Dynamic 3d human-object interactions from videos. *arXiv preprint arXiv:2108.08420*, 2021. 2
- [44] Tao Yu, Zerong Zheng, Kaiwen Guo, Pengpeng Liu, Qionghai Dai, and Yebin Liu. Function4d: Real-time human volumetric capture from very sparse consumer rgbd sensors. In *Proceedings of the IEEE/CVF conference on computer vision and pattern recognition*, pages 5746–5756, 2021. 2, 5
- [45] Zehao Yu, Songyou Peng, Michael Niemeyer, Torsten Sattler, and Andreas Geiger. Monosdf: Exploring monocular geometric cues for neural implicit surface reconstruction. *Advances in neural information processing systems*, 35:25018–25032, 2022. 1, 2
- [46] Juze Zhang, Haimin Luo, Hongdi Yang, Xinru Xu, Qianyang Wu, Ye Shi, Jingyi Yu, Lan Xu, and Jingya Wang. Neuraldome: A neural modeling pipeline on multi-view human-object interactions. In *Proceedings of the IEEE/CVF Conference on Computer Vision and Pattern Recognition*, pages 8834–8845, 2023. 2, 5
- [47] Jason Y Zhang, Sam PePose, Hanbyul Joo, Deva Ramanan, Jitendra Malik, and Angjoo Kanazawa. Perceiving 3d human-object spatial arrangements from a single image in the wild. In *Computer Vision—ECCV 2020: 16th European Conference, Glasgow, UK, August 23–28, 2020, Proceedings, Part XII 16*, pages 34–51. Springer, 2020. 1, 2
- [48] Lvmin Zhang, Anyi Rao, and Maneesh Agrawala. Adding conditional control to text-to-image diffusion models. In

Proceedings of the IEEE/CVF International Conference on Computer Vision, pages 3836–3847, 2023. [3](#), [1](#)

- [49] Yanqiang Zhang, Lijin Fang, and Chengpeng Li. Generalized deep implicit surface network for image-based three-dimensional object reconstruction. In *2021 China Automation Congress (CAC)*, pages 276–281. IEEE, 2021. [2](#)
- [50] Zerong Zheng, Tao Yu, Yebin Liu, and Qionghai Dai. Pamir: Parametric model-conditioned implicit representation for image-based human reconstruction. *IEEE transactions on pattern analysis and machine intelligence*, 44(6): 3170–3184, 2021. [2](#)